

New inline wideband dynamic semiconductor laser amplifier model

A.J. Lowery

Indexing terms: Semiconductor lasers, Amplifiers

Abstract: The formulation of a new scattering matrix, and the use of a gain compensation term allows the transmission-line laser model, previously described, to simulate both travelling-wave and Fabry-Perot laser amplifiers. The new model's results are in excellent agreement with those of other workers for both static operation of travelling-wave amplifiers and dynamic switching of Fabry-Perot amplifiers. To show the wideband nature of the model, a single-repeater 2 Gbit/s fibre communication system is investigated in both the time and frequency domains.

1 Introduction

Semiconductor laser amplifiers (SLAs) have received considerable attention over the last decade. The simplest class of device is the Fabry-Perot laser amplifier (FPLA), which is merely a Fabry-Perot laser that is operated below threshold, and subject to an optical signal incident on one or more facets. If the device is operated above threshold, it is known as an injection-locked laser, and these are commonly used as stable modulated sources [1, 2]. If the facets are antireflectance (AR) coated then a second class of device is produced: the travelling-wave laser amplifier (TWLA). TWLAs have a nonresonant cavity, and so can provide a virtually flat frequency response over tens of the FPLAs resonant modes [3-7]. At low signal levels, up to 40 dB gain is available, but, higher input signal levels cause gain saturation as the carrier concentration becomes depleted by stimulated emission.

The high bandwidth and low noise of TWLAs has prompted studies into their application as optical preamplifiers [6, 7] and nonregenerative repeaters [8, 9]. Theoretical work predicts that optical preamplifiers can give increased sensitivity over *pin* photodiodes at multi-Gbit/s rates [10-12]. In these systems, a narrow-band optical filter is required to reduce spontaneous emission and beat-noise sources, the latter owing to the square law photodetector.

The FPLA has an implicit filtering action. However, the positions of its passbands are carrier and temperature dependent [13], requiring sophisticated control equipment to maintain tuning to the input signal. The resonant cavity, and the implicit carrier dependence of active region refractive index, gives each passband of the

FPLA an asymmetric frequency response [14-17]. The asymmetry is power dependent, and at high levels leads to optical bistability [18-21]. This suggests possible applications as logic and memory elements in optical computers, although switching times are limited to around the carrier lifetime.

Models are available for the steady-state operation of both FPLAs and TWLAs, and all assume a single-input frequency. A simplification allowing an analytical approach assumes a homogeneous carrier distribution [22, 23]. This is valid only at low-power levels, when spontaneous recombination is dominant. Adams *et al.* developed an analytical expression for axial field distribution that increased their models' accuracy without resorting to numerical computation [24-26]. Marcuse used a numerical approach to include spatial inhomogeneities and also to calculate total noise power [27]. Signal/noise studies of TWLAs are also available (see References 10-12 and 28-30). However, this aspect of amplifier performance is beyond the scope of this paper.

The dynamics of optical switching in FPLAs are considered by Adams [31] and Sharpin and Dangenais [32]. Adams used his previously developed spatial approximation to simplify a numerical simulation of gain switch-up based on the carrier rate equation. Sharpin and Dangenais obtained similar results using a numerical solution of the Van der Pol and carrier rate equations. An interesting equivalent-circuit model was developed by Probert and Carroll [33]; it uses an LCR circuit to model one of the cavity resonances. This is able to mimic Adams' results, although spatial carrier uniformity and operation close to a mode are assumed.

For the amplifier models to be useful they should be capable of accepting modulated input signals as found in communication systems. These signals usually have a bandwidth of several longitudinal-cavity modes, as Fabry-Perot lasers are rarely single-moded. Even if single-mode operation is achieved, the mode will be 'chirped' over a significant bandwidth when the source laser is modulated [13].

Obviously, the steady-state models [22-27] are unable to cope with modulated input signals. Of the dynamic models, only that in Reference 33 can accept signals composed of more than a single frequency. This is because References 31 and 32 use an analytical expression for the transmission coefficient of the cavity as a basis for their analyses, and this expression is valid only at a single frequency. A number of discrete frequencies could be represented by a set of these equations, but computation time would limit the accuracy of this approach. There would also be problems associated with entering the input signals in both the time and the frequency domains.

The model presented in Reference 33 has a wide band-

Paper 6058J (E73), first received 17th November 1987 and in revised form 2nd March 1988.

The author is with the Department of Electrical and Electronic Engineering, University of Nottingham NG7 2RD, United Kingdom

width because it includes a lumped circuit equivalent of the cavity to model the field within the cavity in the time domain. Signals may be input in the time domain and the output signals may be Fourier transformed to the frequency domain in a similar manner to that used in the proposed model. However, the lumped circuit model models the cavity only in the vicinity of one Fabry-Perot resonance. Thus, it could not deal with an input from a multi-mode laser oscillator, or a heavily chirped single-mode laser.

This paper describes a model which is able to cope with a general input signal, as it includes a wide-band cavity model in the time domain. The input may be, for example, an amplitude modulated or frequency modulated carrier, a wide-bandwidth chirped multimode output of a modulated laser oscillator or a wavelength multiplexed signal from a mixture of sources. The input waveform to the amplifier is described as a series of data pulses. This enables wideband inputs to be used, and also inputs from previous models. Thus, the model may be used 'in a line' of models. Such an approach is useful when considering, for example, a repeated communication system. Compatible models of laser oscillators and photodiodes already exist [34-36], and an impulse response model of fibre dispersion is to be developed. Digital filters may be used to model optical filters, although equivalent circuit filters may be more efficient [37].

The transmission-line semiconductor laser amplifier model (TSLAM) that is introduced here is a development of the transmission-line laser model (TLLM) [34-36]. The TLLM is based on a numerical technique for the solution of the field, and diffusion equations known as transmission-line modelling (TLM) [38, 39 and 40]. TLM uses the voltages and currents in networks of transmission lines to mimic electric and magnetic fields, or diffusion potentials and fluxes, depending on the form of the network. Transmission lines are easily modelled on digital computers. In TLM they simply provide a unit delay over a unit distance. This serves to discretise both space and time, dividing the network into nodes the voltages of which are calculated at discrete times. The nodes scatter incident sampled waveforms to give reflected pulses into the lines. These pulses emerge one iteration later to become incident pulses on adjacent nodes and the process repeats. By the correct choice of scattering matrix, many physical problems can be turned into simple and explicit algorithms.

2 Description of the model

Fig. 1 shows the laser amplifier that will be modelled. This is assumed to be a buried heterostructure, with an active region of width w , depth d , and length L . The cavity length is shown divided into four model sections, each with a centrally placed scattering node. The optical wave is assumed to be index guided, and its profile is assumed to be independent of carrier concentration. This allows a one-dimensional model to be used, as transverse variations are ignored by equating the field, over the whole cross-sectional area of the device, to a uniform quasi-TEM field over the active region [34]. The equivalent TEM electric field is then modelled as voltage waves, V_{Lc} and V_{Rc} , propagating on transmission lines between nodes. Subscripts L and R indicate waves travelling left and right, respectively. If the magnitude of these waves is equated to the forward and backward components of the electric field, multiplied by a unity constant m (metres),

then the photon density at a node is given by

$$S = \bar{n}_e (|V_{Lc}^i|^2 + |V_{Rc}^i|^2) / (Z_p h f c m^2) \quad (1)$$

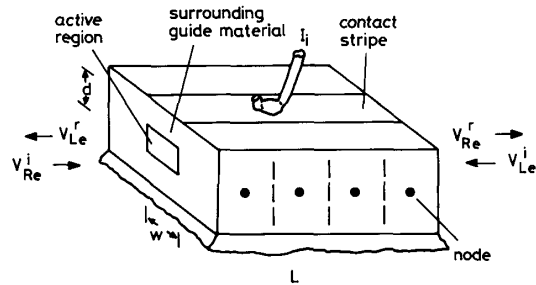


Fig. 1 Laser amplifier showing dimensions and external signals incident on, and reflected from, the facets

The cavity is shown divided into four model nodes

where V_c^i are the waves incident upon the node, Z_p is transverse wave impedance of the TEM wave, and is equal to the impedance of the transmission lines, hf is the photon energy, \bar{n}_e is the group effective index, and c is the vacuum velocity of light.

Similarly, external fields are represented by incident, V_e^i and reflected, V_e^r waves on transmission lines extending from the facets. It is convenient to normalise these fields to the transverse wave impedance rather than the impedance of free space [31]. For example, the incident voltage wave of the left-hand facet, V_{Re}^i , represents an incident power, P_R^i , of

$$P_R^i = |V_{Re}^i|^2 wd / (Z_p m^2) \quad (2)$$

The model for one section is shown in Fig. 2. This includes a field model [38, 39] and a carrier diffusion

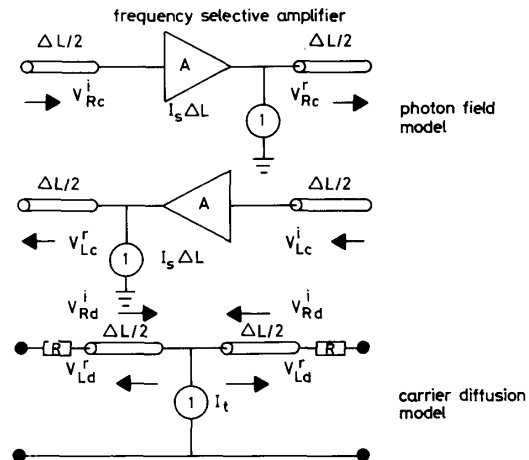


Fig. 2 Transmission line laser and laser amplifier model section including both field and diffusion transmission line models

model [40]. The adjacent nodes are connected by transmission lines which provide distortionless transmission of the waves between the nodes. To discretise time and space, the voltage waveforms on the lines are sampled with a period ΔT at a number s of scattering nodes. The distance between these nodes, ΔL , is arranged so that the linking transmission lines provide exactly ΔT delay to the sampled waves.

As the one-dimensional transmission-line model is dispersionless, then either the group or the phase velocity

along the waveguide must be chosen to link ΔT and ΔL . The choice of group velocity provides the correct longitudinal mode spacing whereas the phase velocity gives the correct absolute frequency [37]. Most commonly the group velocity is used, as absolute frequency is easily corrected with an offset. This gives:

$$\Delta T = \frac{\Delta L}{c} \bar{n}_e \quad (3)$$

To give a realistic computation time, the timestep can be much larger than that governed by the Nyquist sampling limit, as modelled bandwidth is much less than the optical frequency [34]. Usually, it is chosen to give about twenty nodes along the cavity, and interestingly, this gives a modelled bandwidth of the same number of longitudinal modes.

The carrier concentration at a node is equated to the voltage on the nodes of the diffusion model, divided by a unity constant b ($V \text{ cm}^3$). Current waves, passing along the transmission lines linking the nodes, represent diffusion of carriers [40]. The voltage waves representing carrier concentration may be modulated by a current source at the node. This represents stimulated emission, spontaneous emission and carrier injection [36]. The magnitude of this source, I_i , is given by [31]:

$$\frac{I_i z}{b \Delta T} = \frac{I_i}{qwdL} - \frac{N}{\tau_s} - \frac{a\Gamma(N - N_0)}{Z_p h f m^2} [|V_{Lc}^i|^2 + |V_{Rc}^i|^2] \quad (4)$$

where z is the impedance of the transmission lines and all the other parameters are listed in Table 1.

Table 1: Travelling-wave laser amplifier parameters

Symbol	Parameter	Value	Units
λ_0	Nominal input wavelength	1.56	μm
f	Optical frequency	1.923×10^{14}	Hz
h	Plank's constant	6.626×10^{-34}	Js
L	Cavity length	200	μm
d	Active region depth	0.20	μm
w	Active region width	1.50	μm
\bar{n}_e	Group index	4.0	
n_e	Effective index	3.4	
$R_{1,2}$	Facet power reflectivities	0.0	
τ_{ca}	Cavity-air transmission	1.000	
τ_{ac}	Air-cavity transmission coefficient	1.000	
a	Spatial gain per unit inversion	5.0×10^{-16}	cm^2
Γ	Confinement factor	0.5	
N_0	Transparency carrier density	1.0×10^{18}	cm^{-3}
τ_s	Carrier lifetime	4.0	ns
β	Spontaneous emission coupling	0.0	
ΔT	Model timestep	2.4242×10^{-13}	s
s	Number of sections	11	
b	Band number	43	
I_i	Injection current (2 kA/cm^2)	6	mA
Z_p	Cavity wave impedance	130.447	Ω
q	Electronic charge	1.602×10^{-19}	C

This current splits between the two longitudinal directions. Resistors can be used to couple the nodes giving scattering at the node boundaries representing diffusion. Their value is related to the diffusion constant, D , by

$$R = (\Delta L)^2 / (2D \Delta T) \quad (5)$$

In this paper, their value is set to infinity, as diffusion is neglected in the comparisons. This means that the reflected voltage pulses into the transmission lines, V_d^i are perfectly reflected at the node boundaries to become incident pulses on the node, V_d^i one timestep later. Thus the diffusion modes are independent, and the transmission lines serve only to store charge, rather than to transport it

between nodes. For reference, a detailed description of the scattering process can be found in Reference 36.

The field model nodes include frequency selective amplifiers, A . These represent material gain in the cavity and the frequency dependence of that gain [34]. The filter networks inside the amplifiers are modelled by transmission-line stubs [37], representing inductors and capacitors. Both the magnitude and the frequency dependence of the amplifiers is governed by the local carrier concentration. The stimulated emission rate is calculated from the gain and the local field intensity. The cross-coupling of the field and diffusion models is analogous to the coupling between the photon and carrier density rate equations. Indeed, the TLLAM can be thought of as solving the rate equations for a bandwidth of s modes, at s nodes along the cavity. For comparison, Marcuse [27] uses 99 discrete modes bandwidth with 11 longitudinal calculation points. The fundamental difference is that his model gives the photon density for each mode, rather than the resultant optical field for all modes, from which a continuous spectrum may be obtained by a Fourier transform.

Spontaneous emission noise is represented by filtered random current sources* at every node. These are analogous to the current density term in the classical representation of this noise [41], and so inject noise in and around the resonant modes of the cavity and external hardware. This is particularly useful when comparing FPLAs to TWLAs on noise terms, though further study of this is beyond the scope of this paper. For completeness, the magnitude of these sources is

$$\tilde{I}_s^2 = 2m^2 \beta N h f s / (\Delta L Z_p \tau_s) \quad (6)$$

where all the symbols are as defined in Table 1.

As before, the current is split between both directions. However, the current entering the (matched) amplifier is considered to be lost.

In the first TLLMs, the end facets were represented by resistive terminations chosen to provide the correct facet reflectivity. Later TLLMs use a stub-attenuator (SA) facet model to allow laser chirp to be incorporated into the model without introducing instabilities [35]. For the model to accept external input signals, to enable SLAs to be studied, a new facet model is required. This should incorporate a SA model, to allow bistability to be shown. The principal of the stub attenuator model is that the input impedance of a half iteration timestep stub may be matched to that of a small extension to the cavity length. This extension represents the change in phase length of the cavity, owing to carrier-induced modulation of its index [13]. As energy is conserved in the stub, an attenuator is used to represent the facet reflectivity, and this attenuates waves that are reflected from the stub. External fields could be modelled as voltages added to the end of the stub. However, this creates two problems: the input frequency response would be stub dependent, and the stub, being one half of one timestep long, would introduce a mismatch in sampling times. The solution is to add the external input after the stub, at the same position as the attenuator. The phase delay of the cavity will be maintained if the output is also sampled after the opposite end's stub. Fig. 3 shows the signal flow in such an arrangement for one facet. S_s is the stub scattering matrix, which is related to the cavity impedance, Z_p , and

* Lowery, A.J.: 'Representation of spontaneous emission in multilongitudinal-mode semiconductor laser models based on the transmission-line modelling technique' to be published

the stub impedance, Z_s , by

$$\begin{bmatrix} V_f^i \\ V_s^i \end{bmatrix} = \frac{1}{Z_s + Z_p} \begin{bmatrix} (Z_s - Z_c) & 2Z_c \\ 2Z_s & (Z_c - Z_s) \end{bmatrix} \begin{bmatrix} V_c^i \\ V_s^i \end{bmatrix} \quad (7)$$

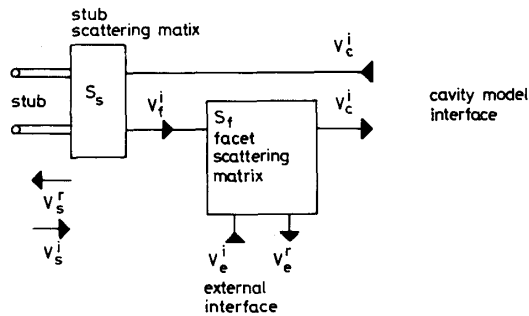


Fig. 3 Signal flow graph for a laser amplifier facet model

S_f is the scattering graph representing the Fresnel reflection and transmission at the facet, and is given by

$$\begin{bmatrix} V_c^r \\ V_e^r \end{bmatrix} = \begin{bmatrix} \rho_{cc} & \tau_{ac} \\ \tau_{ca} & \rho_{aa} \end{bmatrix} \begin{bmatrix} V_f^i \\ V_e^i \end{bmatrix} \quad (8)$$

Where: τ_{ac} is the field transmission coefficient from air to cavity, τ_{ca} is the field transmission coefficient from cavity to air, ρ_{aa} is the field reflection coefficient from air to air, ρ_{cc} is the field reflection coefficient from cavity to cavity.

By inspection of Fig. 2, the matrices may be combined into a single 3×3 scattering matrix, S_i

$$\begin{bmatrix} V_c^r \\ V_e^r \\ V_s^r \end{bmatrix} = \begin{bmatrix} \rho_{cc} \left(\frac{Z_s - Z_c}{Z_s + Z_c} \right) & \tau_{ac} & \rho_{cc} \left(\frac{2Z_c}{Z_s + Z_c} \right) \\ \tau_{ca} \left(\frac{Z_s - Z_c}{Z_s + Z_c} \right) & \rho_{aa} & \tau_{ca} \left(\frac{2Z_c}{Z_s + Z_c} \right) \\ \left(\frac{Z_s}{Z_s + Z_c} \right) & \phi & \left(\frac{Z_c - Z_s}{Z_s + Z_c} \right) \end{bmatrix} \begin{bmatrix} V_c^i \\ V_e^i \\ V_s^i \end{bmatrix} \quad (9)$$

This is easily verified by considering the situations of an infinite stub impedance, and a zero external input. In these cases, the matrix reduces to that for a simple mismatch between air and cavity, and secondly, the SA model described in Reference 35.

3 Steady-state simulation of TWLA

The simulation of a travelling-wave laser amplifier provides a simple test for the model, the results of which can be compared with analytical formulas. The test involves injection of a single frequency into the rear facet. This is chosen to coincide with the peak of the gaincurve that is itself at a fixed frequency for this simulation. In practical devices the position of the peak is carrier dependent [25], and this effect may be included in the model [36]. The model parameters are given in Table 1. Although these values do not include attenuation or spontaneous emission, they do not allow direct comparison with Fig. 1 in Reference 24. For each input power, the carrier concentration in the model is initially set to the expected steady-state value. The model then iterates until a near steady-state is reached. The output power is then calculated from the mean-square of the optical output field. A plot of steady-state gain and output power against input power is shown in Fig. 4. Also plotted are the solutions to eqn. 10 in Reference 24.

The model shows a lower than expected small-signal

gain. However, this is easily explained. It is a consequence of the Taylor series expansion of the exponential gain term [34]. The theoretical small signal (maximum) gain is given by

$$G_{th} = \exp \left[a\Gamma L \tau_s \left(\frac{I_i}{qdWL} - \frac{N_0}{\tau_s} \right) \right] \quad (10)$$

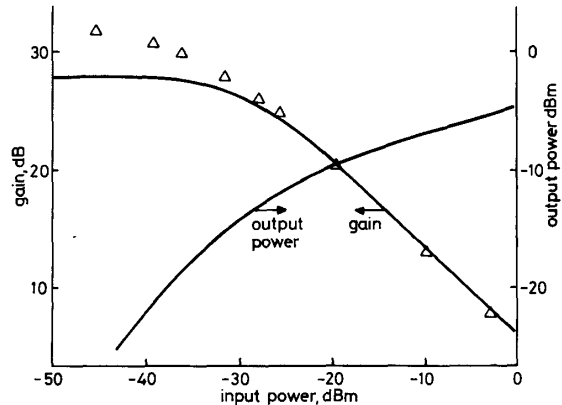


Fig. 4 Gain and output power against input power in the steady-state simulation of the TWLA

Triangles indicate analytical results

whereas in the model the small-signal gain is

$$G_m = \left(1 + \frac{a\Gamma L \tau_s}{2s} \left(\frac{I_i}{qdWL} - \frac{N_0}{\tau_s} \right) \right)^{2s} \quad (11)$$

thus the two gains are related by

$$G_m = \left(1 + \frac{\ln(G_{th})}{2s} \right)^{2s} \quad (12)$$

where the parameters are as defined in Table 1.

Substitution into eqns. 10 and 11 gives gains of 32.5 dB and 28.0 dB, respectively, the latter being an agreement with the numerical results. Examination of eqn. 12 shows that accuracy could be achieved in two ways: by increasing the number of model sections, or by precompensating for the lack of gain using this equation. As the modelling time is proportional to the square of the number of sections, the latter option is preferable. This is reinforced by studies of the FPLA, detailed in the next section, which show that small inaccuracies in cavity gain (1%) can give large errors in the delay time to turn-on (50%). A compensated gain factor can be calculated using eqn. 12. The results of new simulations including this factor show complete agreement with the analytical solution.

4 Dynamic simulations of FPLA

As the model is primarily dynamic it is better suited to the simulation of transient effects than to steady-state situations where any transient due to the initial conditions of the model parameters would have to settle. For this reason, the FPLA is modelled dynamically. The modelled laser parameters, where different from Table 1, are given in Table 2. The operating variables are: the initial input power, final output power, and detuning.

For easy comparison with other works [31-33], the saturation intensity is introduced:

$$I_s = \frac{hc}{\Gamma a \tau_s \lambda_0} \quad (13)$$

Table 2: Additional parameters for the FPLA

Symbol	Parameter	Value	Units
$R_{1,2}$	Facet power reactivities	0.3	
τ_{ca}	Cavity-air transmission coefficient	0.836	
τ_{ac}	Air-cavity transmission coefficient	0.836	
ρ_{cc}	Cavity-cavity reflection coefficient	0.547	
ρ_{aa}	Air-air reflection coefficient	0.000	
a	Spatial gain per unit inversion	2.5×10^{-18}	cm^2
α_{sc}	Attenuation per unit length	25	cm^{-1}
τ_c	Carrier lifetime	2.0	ns
β	Spontaneous emission coupling	0.0	
ΔT	Model timestep	1.7777×10^{-13}	s
s	Number of sections	15	
b	Band-number	34	
I_i	Injection current	7.92	mA
α	Linewidth enhancement factor	10	

For this device, I_s is 512980 W/cm^2 which, when multiplied by the active cavity cross-sectional area, gives a saturation power P_s of 1.539 mW . The dependence of refractive index on carrier concentration is defined by the linewidth enhancement factor, α , given by

$$\alpha = -\frac{dn_a}{dN} \cdot \frac{4\pi}{\lambda_0 a} \quad (14)$$

n_a is the refractive index of the active layer of the waveguide. In comparison, Adams defines his refractive index dependence in terms of effective refractive index using the symbol b , where

$$b = -\frac{dn_e}{dN} \cdot \frac{4\pi}{\lambda_0 a} \quad (15)$$

Westbrook provides a relation between eqns. 14 and 15, using a dilution factor, commonly set to the value of the confinement factor [42]. Thus,

$$b = \Gamma \alpha \quad (16)$$

Adams sets $b = 5$ in his paper, which gives $\alpha = 10$. This is almost twice the commonly accepted value, of around 5.6 [13]. However, to enable comparison with Adams' work, his value of α will be used.

The initial input power, i.e. at zero time and before, sets the initial carrier concentration N_i . For zero initial input power and an unsaturated material gain per unit length of g_0

$$N_i = \frac{g_0}{a} + N_0 \quad (17)$$

For single frequency operation, the frequency difference between the input signal and the centre of a mode, Δf , is expressed as the detuning parameter, δ , which is normalised to the free-spectral range of the Fabry-Perot resonances by

$$\delta = \pi \left(\frac{2 \Delta f \bar{n}_e L}{c} \right) \quad (18)$$

A negative value of δ indicates that the input frequency is below a resonance. It is important to set the peak of the gain curve to this frequency, as even small errors in gain integrate up to give a large error in delay time. The delay time, t_d , defined as the time between the step increase in power and the switch-up spike and can be normalised to the carrier lifetime, which is 2 ns.

The delay time, the peak output, and the steady-state output power are the important characteristics of device behaviour. A series of model runs have been performed to find the above, for several input-powers and three detunings. At the first iteration, a step rise in input power is injected into the device in the form of a sine wave. The initial carrier concentration is set by eqn. 7 for a unsatu-

rated gain of 95% of the threshold gain. This requires a bias current of 98% of threshold, to maintain it for zero input power. With the onset of the step, the carrier concentration begins to fall. The refractive index consequently rises, lowering the Fabry-Perot resonance frequencies towards the input frequency. The effective signal gain is therefore increased, and the output power rises to a peak. This peak occurs when the resonance frequency equals the signal frequency and, because of the high rate of stimulated recombination, is short lived. The output power then settles to a stable, steady-state, value, with the resonance frequency below the signal frequency. A decrease in output power will increase the carrier concentration, moving the resonance frequency upwards, towards the signal frequency, so restoring the output power. Thus, this high-gain state is stable. Fig. 5 shows

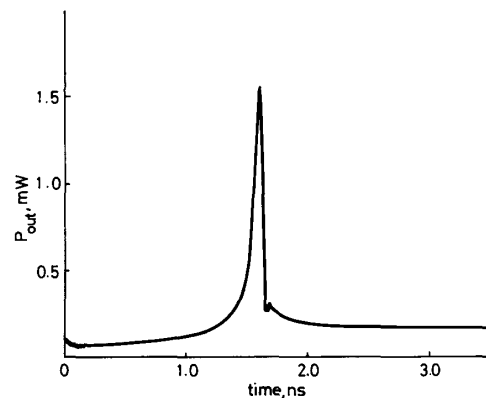


Fig. 5 Transient response of the FPLA during switch-up

A normalised input power 0.0465 is applied at zero time
Initial input is zero
Detuning is $\pi/4$

the switch-up transient when the device is subject to an incident beam of $71.428 \mu\text{W}$, with a detuning of $-\pi/4$. This trace has the same features as Fig. 2 of Reference 31, except for a slight ripple after the power step, and a clipped peak. The former occurs because of Lorentzian broadening of the sine-wave at the turn-on transient, the latter is because of averaging procedure used to convert optical field into power.

Fig. 6 shows the delay times of several simulations plotted with the results of Adams [31]. Each curve represents a different detuning. As expected, the greater the detuning, the larger the delay. The models are in excellent agreement, but this was achieved only after the gain correction factor was included. Small errors in gain concatenate to large errors in delay time, Fig. 7 compares Adams' results for peak and steady-state powers to those of the TSLAM. The steady-state powers for all detunings are also in excellent agreement; the peak powers for the TSLAM are around 20% too low. Again, this is a consequence of the averaging procedure clipping the very sharp peaks of the transients.

5 Repeated communication system simulation

The results of Sections 3 and 4 show that the transmission-line laser amplifier model operates as expected on narrowband signals. The wideband nature of the model will now be demonstrated using a repeated communication system as an example. Fig. 8 shows such a system comprising a semiconductor laser oscillator, modulated by a current waveform, a long length of fibre

with tapered ends to couple to the lasers, a laser amplifier supplied with a bias current, a second long length of fibre, and a *pin* photodiode providing a photocurrent output.

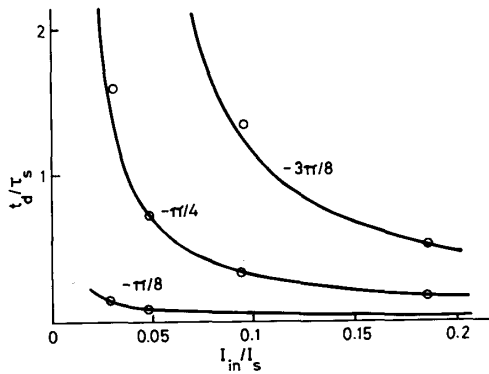


Fig. 6 Time delay to the switching peak as a function of normalised input for the FPLA
 — from Reference 31
 ○○ TLSLAM
 The labelling parameter is detuning

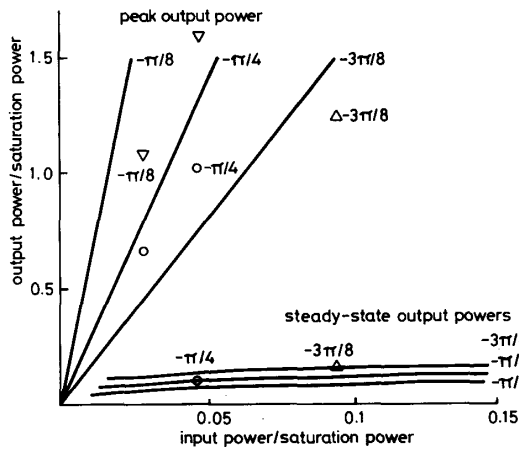


Fig. 7 Peak and steady-state output against input power
 — Adams' results
 △△△ TLSLAM
 ○○○ TLSLAM
 ▽▽▽ TLSLAM

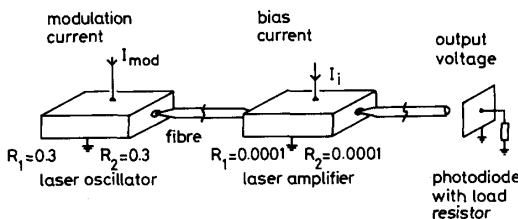


Fig. 8 Single-repeater optical communication system to be modelled

The laser oscillator model converts a modulation current waveform into an optical waveform. It is identical to the laser amplifier model, except that a modulation waveform is included to periodically drive the device above threshold. The device parameters are as in Table 2, with the addition of a spontaneous emission coupling

factor of 0.00001, a modulation period of 500 ps, a current pulse width of 400 ps, a bias current of 5 mA, and a pulse current of 20 mA. The bias level is required to ensure a fast and even pulse response to the data word transmitted (1101). The optical waveform is in the form of a data file of 10000 samples. The separate simulation of oscillator, then amplifier is possible only if backward-travelling waves in the fibre are ignored. If a detailed study of noise is required then the two models may be run simultaneously. Fig. 9 shows the optical power

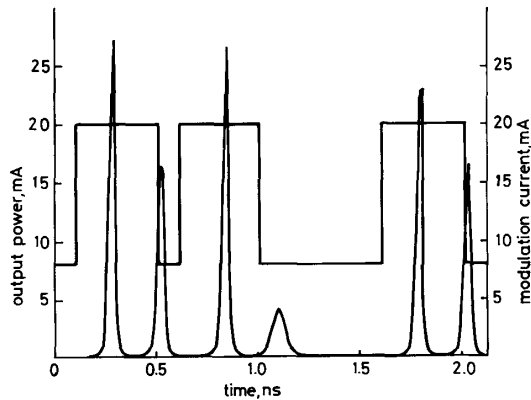


Fig. 9 Modulation response of the laser oscillator
 The rectangular trace is the modulation current waveform

response of the laser. The relaxation oscillations of the device produce two optical pulses per data bit, showing the possibility of higher speed modulation. The spectrum of the first two optical pulses is shown in Fig. 10, and is

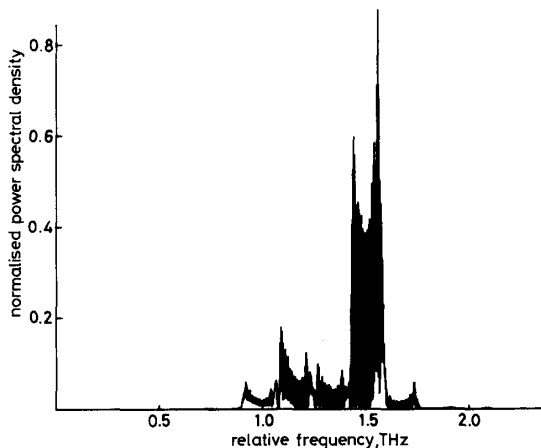


Fig. 10 Spectrum of the first two optical pulses produced by the laser, and shown in Fig. 9

composed of five modes. Each mode has the 'rabbit ear' form, indicating laser chirp [13], merging it with adjacent modes. The degree of chirp of a single pulse is consistent with the analytical formula given in Reference 13. Transforming over two pulses produces an interference effect in the frequency domain, giving a solid appearance to the plot.

The fibre is considered to be dispersionless in this example. This allows a simple attenuator to be used as a fibre model. The fibre loss, including diffraction coupling

losses into the laser, is set to 30 dB. This would give a fibre length of approximately 150 km at 1550 nm [43]. The data from the fibre model is passed to a travelling wave laser amplifier model, which optimistically good facet reflectivities of 0.01% [9]. The other parameters are in Table 2, except the spontaneous emission coupling factor which is the same as the oscillator's. The laser is biased at 12 mA, giving a theoretical gain, neglecting internal attenuation, of 30 dB. Internal attenuation reduces the gain by about 2 dB. The gain spectrum for zero input power is plotted in Fig. 11. This has a small

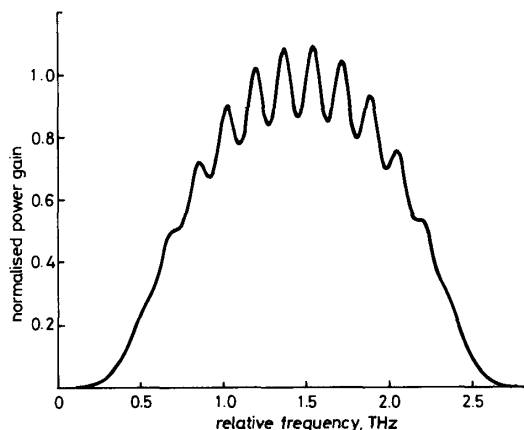


Fig. 11 Power gain frequency dependence of the TWLA model
Ripple magnitude = 1.07 dB

(1.07 dB) ripple, as predicted in Reference 9, allowing the device to be classed as a true travelling-wave amplifier. The amplifier bandwidth is truncated owing to the small model bandwidth. The gain is, however, believed to be accurate around its peak level.

The amplified pulse train is plotted in Fig. 12, and shows good reproduction of the input pulses. However,

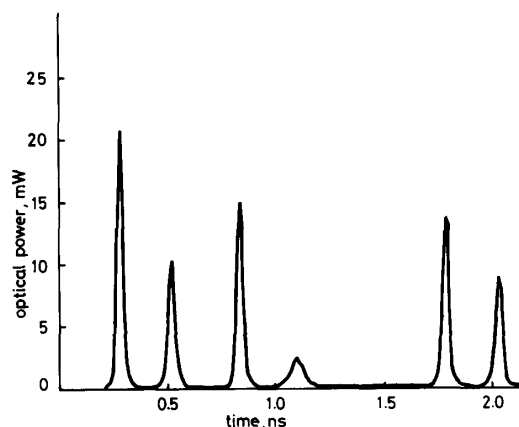


Fig. 12 Optical pulse power after amplification

the third optical pulse is smaller than expected. Investigations indicate that this is owing to reduced gain, as a consequence of carrier depletion after the first pulse. A Fourier transform of the amplifier output is given in Fig. 13. This shows that the amplifier has added little out of band noise, and has a near-flat frequency response.

The output waveform from the amplifier model is piped to a second fibre model, with identical character-

istics to the first. The attenuated waveform is then input into a photodiode model. This rectifies the optical waveform, and then filters it using a first-order RC network,

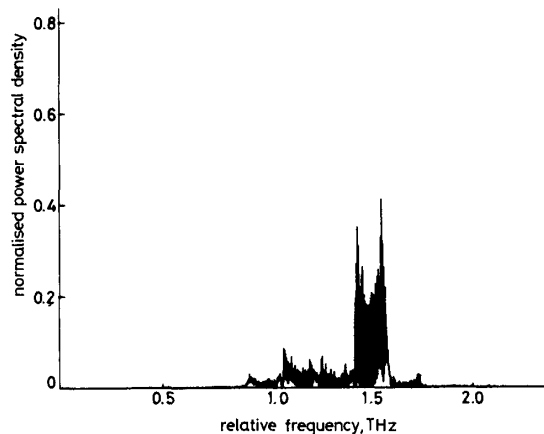


Fig. 13 Spectrum of the first two optical pulses after amplification
Same scaling as Fig. 10

again modelled with transmission lines [36]. The filter represents the combined effects of the photodiode depletion capacitance (4 pF), and the receiver's input impedance (50 Ω). The photodiode responsivity is 0.5 A/W. The filter output is resampled to give a larger timestep (2 ps), suitable for use in receiver circuit models, based on standard packages. The baseband waveform produced is plotted in Fig. 14, and its transform in Fig. 15. It can be

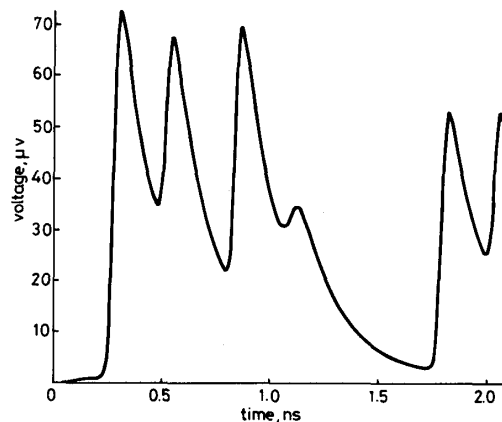


Fig. 14 Photodiode output voltage into a 50 Ω load

seen from Fig. 14 that the data pulses could be recovered using a decision threshold at 25 μ V. This plot also shows the possibility of waveform shaping to obtain a larger threshold, and so a better error rate. A feature of this model is that the photodiode output waveform may be passed to standard circuit analysis packages for filter optimisation.

Finally, the numerical efficiency of the model must be considered. For a bandwidth of 15 modes, with 15 sections, the computation time was 14 min. per laser ns using a 32016-based machine with maths co-processor. If the comparison in Reference 34 is followed, then a 15 discrete-mode rate equation model with a similar number of sections would require 4 min. per laser ns. However,

such a model could not be termed wideband, and would have little possibility of modelling noise effects. It would also ignore phase, making it difficult to add external

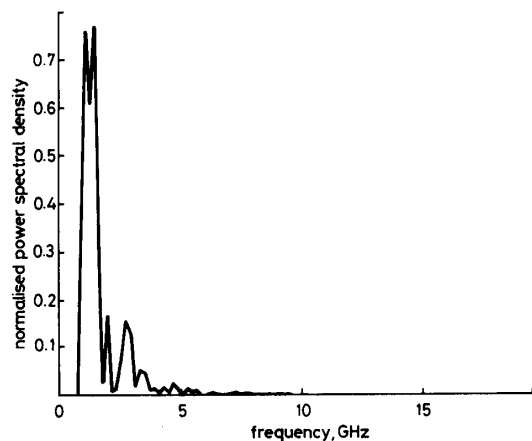


Fig. 15 Power spectrum of the photodiode output

optical components to the simulation. Thus, if for flexibility reasons only, it is beneficial to use the TLSLAM.

6 Conclusions

With the addition of a simple scattering matrix and a gain compensation term, the transmission-line laser model is able to simulate semiconductor laser amplifiers successfully. Steady-state tests on a TWLA showed that for high gains, a correction to the Taylor series representation of material gain was required. The importance of this correction was highlighted in dynamic simulations of switching of an FPLA. A small inaccuracy in gain leads to a large error in the delay-time to the switch-on spike. With the correction term, the results were in exact agreement with the semi-analytical simulations of Adams.

The model was then used for a single-repeater fibre optic communication system operating at 2 Gbit/s. A laser amplifier model, modulated above threshold, provided an optical signal. This was attenuated with a dispersionless fibre model before being injected into a true travelling-wave laser amplifier model. The amplification introduced a small amount of pulse-height distortion and broad-band noise. The further-attenuated signal was finally detected by a photodiode model that showed that digital signal recovery was possible, using a fixed threshold of 25 μ V. It was proposed that the bit error rate of the signal could be improved using optimised filters, and that the modelled photodiode signal could be passed to circuit-simulation programs for this optimisation.

A rough comparison with the speed of a proposed 15 discrete mode, 15 section, rate equation, model indicated that the TLSLAM would be about a factor of four slower. However, the discrete-mode model could not be called wideband, and could not be easily modified to cover new physical problems. Future areas of research suited to the TLSLAM include: noise aspects of amplification including the effects of external components on the noise figure, amplification of multiple signals (WDM and Duplex) and assessments of amplifier phase linearity.

7 Acknowledgments

I would like to thank Professor T.R. Rowbotham and Dr. M.J. Adams, both of British Telecom Research

Laboratories, England, for discussions on the above topics.

8 References

- MOGENSEN, F., OLESEN, H., and JACOBSEN, G.: 'Locking conditions and stability properties for a semiconductor laser with external light injection', *IEEE J. Quantum Electron.*, 1985, **QE-21**, pp. 784-793
- OTSUKA, K., and TARUCHA, S.: 'Theoretical studies on injection locking and injection induced modulation of laser diodes', *ibid.*, 1981, **QE-17**, pp. 1515-1521
- SAITOH, T., and MUKAI, T.: 'Broadband 1.5 μ m GaInAsP travelling-wave laser amplifier with high-saturation output power', *Electron. Lett.*, 1987, **23**, 218-219
- WEBB, R.P., and DEVLIN, W.J.: 'Travelling-wave laser amplifier experiments at 1.5 μ m', *ibid.*, 1984, **20**, pp. 706-707
- EISENSTEIN, G., JOHNSON, R.M., LINKE, R.A., BURRUS, C.A., KOREN, U., WHALEN, M.S., and HALL, K.L.: 'Gain measurements of InGaAsP 1.5 μ m optical amplifiers', *ibid.*, 1983, **19**, pp. 295-297
- O'MAHONY, M.J., MARSHALL, I.W., WESTLAKE, H.J., and STALLARD, W.G.: 'Wideband 1.5 μ m optical receiver using a travelling-wave laser amplifier', *ibid.*, 1986, **22**, pp. 1238-1240
- MARSHALL, I.W., SPIRIT, D.M., and O'MAHONY, M.J.: 'Picosecond pulse response of a travelling-wave semiconductor laser amplifier', *ibid.*, 1987, **23**, pp. 818-819
- STEELE, R.C., and MARSHALL, I.W.: '100 Mbit/s PSK heterodyne experiment using a travelling-wave laser amplifier', *ibid.*, 1987, **23**, pp. 296-297
- EISENSTEIN, G., JOHNSON, B.C., and RAYBON, G.: 'Travelling-wave optical amplifier at 1.3 μ m', *Electron. Letts.*, 1987, **23**, pp. 1020-1022
- FYE, D.M.: 'Practical limitations on optical amplifier performance', *IEEE J. Lightwave Tech.*, 1984, **LT-2**, pp. 403-406
- MUKAI, T., YAMAMOTO, Y., and KIMURA, T.: 'S/N and error rate performance in AlGaAs semiconductor laser preamplifier and linear repeater systems', *IEEE Trans. Mic. Theory & Tech.*, 1982, **MTT-30**, pp. 1548-1556
- YAMAMOTO, Y.: 'Noise and error rate performance of semiconductor laser amplifiers in PCM-IM optical transmission systems', *IEEE J. Quantum Electron.*, 1980, **QE-16**, pp. 1073-1081
- OSINSKI, M., and BUUS, J.: 'Linewidth broadening factor in semiconductor lasers - An overview', *ibid.*, 1987, **QE-23**, pp. 9-29
- KOBAYASHI, K., NISHIMOTO, H., and LANG, R.: 'Experimental observation of asymmetric detuning characteristics in semiconductor laser injection locking', *Electron. Letts.*, 1982, **18**, pp. 55-57
- GOLDBERG, L., TAYLOR, H.F., and WELLER, J.F.: 'Locking bandwidth asymmetry in injection-locked GaAlAs lasers', *ibid.*, 1982, **18**, pp. 986-987
- NAKAI, T., ITO, R., and OGASAWARA, N.: 'Asymmetric frequency response of semiconductor laser amplifiers', *Jpn. J. Appl. Phys.*, 1982, **21**, pp. L680-L682
- KURWAHARA, H., CHIKAMA, T., and NAKAGAMI, T.: 'Tuning characteristics of optical amplification in 1.5 μ m InGaAsP/InP lasers', *Electron. Letts.*, 1983, **19**, pp. 295-297
- OTSUKA, K., and KOBAYASHI, S.: 'Optical bistability and nonlinear resonance in a resonant-type semiconductor laser amplifier', *ibid.*, 1983, **19**, pp. 262-263
- NAKAI, T., OGASAWARA, N., and ITO, R.: 'Optical bistability in a semiconductor laser amplifier', *Jpn. J. Appl. Phys.*, 1983, **22**, pp. L310-L312
- OTSUKA, K., and IWAMURA, H.: 'Theory of multistability and chaos in a resonant-type semiconductor laser amplifier', *Phys. Rev. A*, 1983, **28**, pp. 3153-3155
- MOGENSEN, F., JACOBSEN, G., and OLESEN, H.: 'Light intensity pulsations in an injection-locked semiconductor laser', *Opt. & Quant. Electron.*, 1984, **16**, pp. 183-186
- OTSUKA, K., and IWAMURA, H.: 'Analysis of a multistable semiconductor light amplifier', *IEEE J. Quantum Electron.*, 1983, **QE-19**, pp. 1184-1186
- BUUS, J., and PLASTOW, R.: 'A theoretical and experimental investigation of Fabry-Perot semiconductor laser amplifiers', *ibid.*, 1985, **QE-21**, pp. 614-617
- ADAMS, M.J., COLLINS, J.V., and HENNING, I.D.: 'Analysis of semiconductor laser optical amplifiers', *IEE Proc. J., Optoelectron.*, 1985, **132**, pp. 58-63
- HENNING, I.D., ADAMS, M.J., and COLLINS, J.V.: 'Performance predictions from a new optical amplifier model', *IEEE J. Quantum Electron.*, 1985, **QE-21**, pp. 609-613

- 26 ADAMS, M.J., WESTLAKE, H.J., O'MAHONY, M.J., and HENNING, I.D.: 'A comparison of active and passive optical bistability in semiconductors', *ibid.*, 1985, **QE-21**, pp. 1498-1504
- 27 MARCUSE, D.: 'Computer model of an injection laser amplifier', *ibid.*, 1983, **QE-19**, pp. 63-73
- 28 ARNAUD, J.: 'Theory of spontaneous emission in gain-guided laser amplifiers', *Electron. Letts.*, 1983, **19**, pp. 798-800
- 29 SIMON, J.C.: 'Semiconductor laser amplifier for single mode optical fiber communications', *J. Opt. Commun.*, 1983, **4**, pp. 51-62
- 30 SCHUNK, N., and PETERMANN, K.: 'Noise analysis of injection-locked semiconductor injection lasers', *IEEE J. Quantum Electron.*, 1986, **QE-22**, pp. 642-650
- 31 ADAMS, M.J.: 'Time dependant analysis of active and passive optical bistability in semiconductors', *IEE Proc. J., Optoelectron.*, 1985, **132**, pp. 343-348
- 32 SHARPIN, W.F., and DANGENAI, M.: 'Dynamics of optically switched bistable diode laser amplifiers', *IEEE J. Quantum Electron.*, 1987, **QE-23**, pp. 303-308
- 33 PROBERT, P.J., and CARROLL, J.E.: 'Modelling bistability in injection-laser amplifiers using lumped-circuit models', *IEE Proc. J., Optoelectron.*, 1987, **134**, pp. 295-302
- 34 LOWERY, A.J.: 'A new dynamic semiconductor laser model based on the transmission line modelling method', *ibid.*, 1987, **134**, pp. 281-289
- 35 LOWERY, A.J.: 'A model for multimode picosecond dynamic laser chirp based on the transmission line laser model', *ibid.*, 1988, **135**, pp. 126-132
- 36 LOWERY, A.J.: 'A study of the static and multi-Gigabit dynamic effects of gain spectra carrier dependence in semiconductor lasers using a transmission line laser model', *IEEE J. Quantum Electron.*, 1988, **QE-24**, pp. unknown
- 37 JOHNS, P.B., and O'BRIEN, M.: 'Use of the transmission line modelling (t.l.m.) method to solve non-linear lumped networks', *Radio & Electron. Eng.*, **50**, pp. 59-70
- 38 JOHNS, P.B., and BEURLE, R.L.: 'Numerical solution of 2-dimensional scattering problems using a transmission line matrix', *IEE Proc.*, 1971, **118**, pp. 1203-1208
- 39 JOHNS, P.B.: 'The solution of inhomogeneous waveguide problems using a transmission-line matrix', *IEEE Trans. Mic. Theory & Tech.*, 1974, **MTT-22**, pp. 209-215
- 40 JOHNS, P.B.: 'A simple explicit and unconditionally stable numerical route for the solution of the diffusion equation', *Journal of Numerical Methods in Engineering*, 1971, **11**, pp. 1307-1328
- 41 MARCUSE, D.: 'Classical derivation of the laser rate equation', *IEEE J. Quantum Electron.*, 1983, **QE-19** pp. 1228-1231
- 42 WESTBROOK, L.D.: 'Measurements of dg/dN and dn/dN and their dependence on photon energy in $\lambda = 1.5 \mu\text{m}$ InGaAs laser diodes', *IEE Proc. J., Optoelectron.*, 1986, **133**, pp. 135-142
- 43 MIYA, T., TERUNUMA, Y., HOSAKA, T., and MIYASHITA, T.: 'Ultimate low-loss single-mode fibre at $1.55 \mu\text{m}$ ', *Electron. Letts.*, 1979, **15**, pp. 106-108